Journal of Computational and Applied Mathematics 226 (2009) 370–387

Contents lists available at ScienceDirect

Journal of Computational and Applied Mathematics

journal homepage: www.elsevier.com/locate/cam

Analysis of an interface relaxation method for composite elliptic differential equations

P. Tsompanopoulou, E. Vavalis *

University of Thessaly, Department of Computer & Communication Engineering, Glavani Street 37, GR 382 21 Volos, Greece
Center for Research and Technology - Thessaly, Technology Park of Thessaly, GR 385 00 Volos, Greece

ARTICLE INFO

Keywords:
Interface relaxation
Domain decomposition methods
Elliptic partial differential equations

ABSTRACT

The theoretical analysis on both the continuous (differential) and the discrete (linear algebra) levels of an interface relaxation method for solving elliptic differential equations is presented. The convergence of the method for 1-dimensional problems is proved. The region of convergence and the optimal values for the relaxation parameters involved are determined for model problems. Numerical data for 1- and 2-dimensional problems that confirm the theoretical results, exhibit the effectiveness of the method and elucidate its characteristics are presented.

1. Introduction

Interface Relaxation (*IR*), [10–14] appears to be an attractive alternative to the traditional domain decomposition approach, particularly when modeling multiphysics/multidomain problems. The main advantage of the *IR* framework is the fact that it provides enough versatility so that one can freely select:

- the most efficient numerical method for each subproblem naturally defined by either the original problem's multidomain structure or its multiphysics nature.
- the most appropriate condition that accurately models the physical interaction between two different problems that match on a particular interface.

Furthermore, one of the most desirable characteristics of the iterative *IR* schemes is the fact that their rates of convergence only depend on the parameters of the problem itself, the ones related to its decomposition into subproblems and the parameters related to the operator imposed on the interfaces. Their rates of convergence do not depend (or at most it is affected very little) on the parameters associated with the numerical schemes employed for the solution of each subproblem (e.g., number of finite elements).

Collaborating PDE solvers based on interface relaxation have been already proposed [5,7,9,10,8] and have been rather extensively considered for air pollution [16,17], underwater acoustics [1] and gas turbine engine [6,4] related simulations. In addition, interface relaxation appears to be a very promising framework for coupling Finite Element and Boundary Element methods in electromagnetic applications and beyond (see [18] and references within).

A relatively large class of interface relaxation methods have been derived and theoretically analyzed (e.g., [5,8,13, 11,12,14]) for model problems and decompositions. Numerical experiments have been also already presented (see for example [11,12,14]) but most of them are for mainly 1-dimensional problems or simple 2-dimensional ones but with 1-dimensional decompositions. In particular, a collection of ten such *IR* methods is presented in [11] together with an early experimental comparative study on mainly 1-dimensional differential problems. Although recent theoretical and

* Corresponding author at: Center for Research and Technology - Thessaly, Technology Park of Thessaly, GR 385 00 Volos, Greece.
E-mail address: mav@inf.uth.gr (E. Vavalis).

0377-0427/$ – see front matter © 2008 Elsevier B.V. All rights reserved.
doi:10.1016/j.cam.2008.08.021

experimental studies [12,8,9] have shown that the *IR* methods are very effective, it is apparent that the theoretical analysis of these methods is difficult especially when different discretization schemes are used on different subdomains/subproblems. The analysis of *IR* methods is usually carried out either on the continuous or the discrete level and is based on tools from different mathematical areas that range from linear algebra and finite element to discrete and continuous Banach spaces. It is our belief that a combination of different approaches in the theoretical analysis of *IR* methods will provide the insight that is required in order to further exploit the practical use of the *IR* framework.

The main objective of our paper is to theoretically analyze and experimentally investigate and evaluate a new *IR* method, named **GEO** for solving elliptic differential equations. This method is based on a simple geometric contraction mechanism and iterates to relax the values on the interfaces by adding to the old ones a geometrically weighted combination of the normal boundary derivatives of the adjacent subdomains. Specifically, we consider the following iterative relaxation formula on an interface point x

$$u^{(k+1)}(x) = u^{(k)}(x) - \rho\left(\frac{\partial u_L^{(k)}(x)}{\partial \eta} - \frac{\partial u_R^{(k)}(x)}{\partial \eta}\right), \quad k = 1, 2, \ldots \tag{1}$$

where k denotes the iteration step, u the approximation of the solution on the interface point x, and $\frac{\partial u_L}{\partial \eta}$, $-\frac{\partial u_R}{\partial \eta}$ the values of the outward normal derivatives of the computed solution in the two adjacent subdomains. ρ is a relaxation parameter which is motivated by a simple geometric reasoning (presented in the next section) and it is used to accelerate the convergence of the iteration scheme.

The **GEO** method was first briefly proposed in [11], where its derivation can be found together with preliminary 1-dimensional experimental data. A variation of this method has been also considered in [8] where a convergence analysis has been carried out and numerical data are presented. Unfortunately, the rate of convergence of this variation of the method strongly depends on the discretization parameter h and as such violates one of the main principles of interface relaxation. Furthermore, it has been observed that it converges so slowly that it needs preconditioning. In this paper we analyze the **GEO** scheme and prove, for 1-dimensional model problems, that the convergence is independent of h. This independence is clearly confirmed for both 1- and 2-dimensional problems through extensive numerical experiments.

The rest of this paper is organized as follows. In Section 2 we present the formulation of the **GEO** relaxation method and in Sections 3 and 4 we present the convergence analysis on the continuous level and the discrete level respectively. Numerical data can be found in Section 5. They confirm our convergence results and show that they hold for more general problems and decomposition configurations. Our conclusions are given in Section 6.

2. GEO: A geometry based interface relaxation method

Consider the composite differential problem defined by

$$Lu = f \quad \text{in } \Omega \setminus \partial\Omega, \qquad u = u^b \quad \text{on } \partial\Omega \tag{2}$$

where u^b is a prescribed function on the boundary, $\Omega \equiv \cup_{i=1}^{p} \overline{\Omega_i}$ and Ω_i, $i = 1, \ldots, p$, are open sets such that $\cap_{i=1}^{p} \Omega_i = \emptyset$. L is an elliptic differential operator which might be different in each subdomain Ω_i. For the simplicity in the presentation of the convergence analysis given in the next section we restrict ourselves only to Dirichlet boundary conditions on $\partial\Omega$.

As is typical for *IR* methods the above problem can be replaced with the following loosely coupled system of differential problems.

$$\begin{aligned} &L_i u_i = f_i \quad \text{in } \Omega_i, \\ &G_{ij} u = 0 \quad \text{on } (\partial\Omega_i \cap \partial\Omega_j) \setminus \partial\Omega \quad \forall j \neq i, \qquad u = u_i^b \quad \text{on } \partial\Omega_i \cap \partial\Omega, \end{aligned} \tag{3}$$

where for $i = 1, \ldots, p$, L_i, f_i and u_i^b are the restrictions of L, f and u^b respectively on each subdomain Ω_i and G_{ij} is a condition on the interface between subdomains Ω_i and Ω_j which enforces *proper coupling*. This coupling might range from complicated differential operators that preserve certain physical properties or quantities to simple smoothing or jump conditions [10,11].

The formulation of the method can be easily derived for any kind of coupling and it seems that the analysis given next can be also extended with no significant difficulties. Nevertheless, in this study we restrict ourselves to the most common case of smooth global solution for second order differential equations where we only need to impose the continuity of the solution and its first (normal) derivative on the interface lines. In this case the **GEO** method obtains new values on the interface lines by adding to the old ones a geometrically weighted average of the normal boundary derivatives of the adjacent subdomains.

Specifically, let us consider a 1-dimensional case and denote by u_L and u_R the solutions of the differential problems associated with the domain on the left and on the right of an interface point I respectively. Assume that they are equal on I (if not we may take their average on I) but their slopes do not match unless we add a correction term m as is geometrically depicted in Fig. 1. To calculate m we consider the two right triangles IAB and CDI whose heights h_L and h_R are given by multiplying the corresponding tangent (or equivalently the normal derivative) with the base of the triangle. w_L and w_R are the widths assumed for the validity of the slope values S_L and S_R respectively on I. They may be arbitrary selected or play the role of a relaxation parameter that might change dynamically from iteration to iteration. The new interface values can

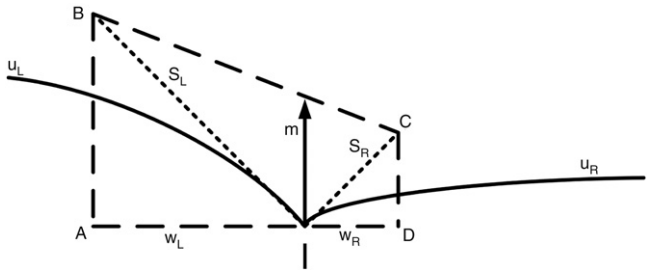

Fig. 1. The smoothing mechanism of the **GEO** interface relaxation method.

be now calculated by adding a weighted average of the heights to the old interface values. One may intuitively view the above smoothing as grabbing the functions u_L and u_R at interface I and stretching them upwards by m until their derivatives become continuous.

Based on the above discussion we can define the **GEO** method, at algorithmic level, for the model problem considered above, by the following iterative scheme:

1. Define for $i = 1, \ldots, p-1$:
$$g_i^i := \left.\frac{u_i^{(k)} + u_{i+1}^{(k)}}{2}\right|_{x=x_i} + \left.\frac{w_i^i w_i^{i+1}}{w_i^i + w_i^{i+1}}\left(-\frac{\mathrm{d}u_i^{(k)}}{\mathrm{d}x} + \frac{\mathrm{d}u_{i+1}^{(k)}}{\mathrm{d}x}\right)\right|_{x=x_i}.$$
2. Choose initial guesses $u_i^{(0)}(x)$ for the solutions on each subdomain Ω_i, $i = 1, 2, \ldots, p$.
3. Define the sequence of subdomain solutions $u_i^{(k)}(x)$, $k = 1, 2, \ldots$, as follows:

$$\begin{array}{lll} & \text{for } i = 2, \ldots, p-1 & \\ L_1 u_1^{(k+1)} = f_1 \quad \text{in } \Omega_1 & L_i u_i^{(k+1)} = f_i \quad \text{in } \Omega_i & L_p u_p^{(k+1)} = f_p \quad \text{in } \Omega_p \\ \left.u_1^{(k+1)}\right|_{x=x_0} = u_1^b & \left.u_i^{(k+1)}\right|_{x=x_{i-1}} = g_{i-1}^{i-1} & \left.u_p^{(k+1)}\right|_{x=x_{p-1}} = g_{p-1}^{p-1} \\ \left.u_1^{(k+1)}\right|_{x=x_1} = g_1^1 & \left.u_i^{(k+1)}\right|_{x=x_i} = g_i^i & \left.u_p^{(k+1)}\right|_{x=x_p} = u_p^b. \end{array}$$

To the best of our knowledge the only known interface relaxation method that shares significant similarities with the **GEO** method is the one proposed and analyzed in [8] for which both the analysis and, to a great extent, the formulation is based on a discrete scheme that arises by using the 5-point star discretization method and $O(h)$ approximation of the normal derivatives involved in the relaxation mechanism. As such the relaxation parameter is a function of the discretization parameter h; it is common to all subdomains and takes no account of the geometric and topological characteristics of the subdomains.

As is clearly seen from both the theoretical analysis and experimental data presented in [8] the convergence rate of this method unfortunately depends on the discretization step h and in fact the rate of convergence slows down quite rapidly as the discretization becomes finer.

3. Convergence analysis on the continuous level

Let us first introduce the required notation for the sequence of values of the solutions, their derivatives and their errors at the interface points as follows

$$u_{i,j}^{(k)} \equiv u_i^{(k)}(x_j), \qquad \mathrm{d}u_{i,j}^{(k)} \equiv \left.\frac{\mathrm{d}u_i^{(k)}}{\mathrm{d}x}\right|_{x=x_j},$$
$$\epsilon_i^{(k)}(x) \equiv u_i^{(k)}(x) - u(x), \qquad \epsilon_{i,j}^{(k)} \equiv u_{i,j}^{(k)} - u(x_j) \quad \text{and} \quad \mathrm{d}\epsilon_{i,j}^{(k)} \equiv \mathrm{d}u_{i,j}^{(k)} - u'(x_j).$$

Please note that for our convergence analysis we only need to consider the error on the interfaces. As can be easily seen, if this error goes to zero, (as $k \longrightarrow \infty$) the g_i^i, $i = 1, \ldots, p-1$ in step 3 of the method (see Section 2) converge to the exact values of the solution on the interfaces and therefore the subdomain solutions $u_i^{(k)}(x)$ converge to the restrictions of the exact solution $u(x)$ in each subdomain i.

We then proceed by obtaining from the iterative relaxation scheme given in Section 2 the following differential problems concerning the error functions associated with the subdomains.

$$\begin{aligned} & L_1 \epsilon_1^{(k+1)}(x) = 0, \quad x \in \Omega_1, \\ & \epsilon_{1,0}^{(k+1)} = 0, \qquad \epsilon_{1,1}^{(k+1)} = \frac{\epsilon_{1,1}^{(k)} + \epsilon_{2,1}^{(k)}}{2} + \rho_1\left(-\mathrm{d}\epsilon_{1,1}^{(k)} + \mathrm{d}\epsilon_{2,1}^{(k)}\right), \end{aligned} \tag{4}$$

for $i = 2, \ldots, p-1$,

$$
\begin{aligned}
&L_i \epsilon_i^{(k+1)}(x) = 0, \quad x \in \Omega_i,\\
&\epsilon_{i,i-1}^{(k+1)} = \frac{\epsilon_{i-1,i-1}^{(k)} + \epsilon_{i,i-1}^{(k)}}{2} + \rho_{i-1}\left(-\mathrm{d}\epsilon_{i-1,i-1}^{(k)} + \mathrm{d}\epsilon_{i,i-1}^{(k)}\right),\\
&\epsilon_{i,i}^{(k+1)} = \frac{\epsilon_{i,i}^{(k)} + \epsilon_{i+1,i}^{(k)}}{2} + \rho_i\left(-\mathrm{d}\epsilon_{i,i}^{(k)} + \mathrm{d}\epsilon_{i+1,i}^{(k)}\right),
\end{aligned} \tag{5}
$$

$$
\begin{aligned}
&L_p \epsilon_p^{(k+1)}(x) = 0, \quad x \in \Omega_p,\\
&\epsilon_{p,p}^{(k+1)} = 0, \qquad \epsilon_{p,p-1}^{(k+1)} = \frac{\epsilon_{p-1,p-1}^{(k)} + \epsilon_{p,p-1}^{(k)}}{2} + \rho_{p-1}\left(-\mathrm{d}\epsilon_{p-1,p-1}^{(k)} + \mathrm{d}\epsilon_{p,p-1}^{(k)}\right),
\end{aligned} \tag{6}
$$

where $\rho_i = \frac{w_i^i w_i^{i+1}}{w_i^i + w_i^{i+1}} > 0$, $i = 1, \ldots, p-1$.

For the convergence analysis that will follow we restrict ourselves to the Helmholtz equation, i.e., we set

$$L_i\phi \equiv -\frac{\mathrm{d}^2\phi}{\mathrm{d}x^2} + \gamma_i^2\phi, \quad \gamma_i \in \mathbb{R}$$

and we make use of the following lemma which can be easily verified.

Lemma 1. *The solution of the boundary value problem*

$$-\frac{\mathrm{d}^2u}{\mathrm{d}x^2} + \gamma^2 u = 0 \quad \textit{in } (a,b), \qquad u(a) = v_1 \quad \textit{and} \quad u(b) = v_2$$

is given by

$$u(x) = \frac{(\mathrm{e}^{\gamma(b-x)} - \mathrm{e}^{-\gamma(b-x)})v_1 + (\mathrm{e}^{\gamma(x-a)} - \mathrm{e}^{-\gamma(x-a)})v_2}{\mathrm{e}^{\gamma(b-a)} - \mathrm{e}^{-\gamma(b-a)}}. \tag{7}$$

Setting $l_i := x_i - x_{i-1}$ and using Lemma 1 and Eqs. (4)–(6) we easily derive the following expressions concerning the error functions at two consecutive iterations:

$$\epsilon_1^{(k+1)}(x) = \frac{\mathrm{e}^{\gamma_1(x-x_0)} - \mathrm{e}^{-\gamma_1(x-x_0)}}{\mathrm{e}^{\gamma_1\ell_1} - \mathrm{e}^{-\gamma_1\ell_1}}\left(\frac{\epsilon_{1,1}^{(k)} + \epsilon_{2,1}^{(k)}}{2} + \rho_1\left(-\mathrm{d}\epsilon_{1,1}^{(k)} + \mathrm{d}\epsilon_{2,1}^{(k)}\right)\right), \tag{8}$$

for $i = 2, \ldots, p-1$,

$$
\begin{aligned}
\epsilon_i^{(k+1)}(x) = \left[\mathrm{e}^{\gamma_i\ell_i} - \mathrm{e}^{-\gamma_i\ell_i}\right]^{-1}\Bigg[&\left(\mathrm{e}^{\gamma_i(x_i-x)} - \mathrm{e}^{-\gamma_i(x_i-x)}\right)\left(\frac{\epsilon_{i-1,i-1}^{(k)} + \epsilon_{i,i-1}^{(k)}}{2} + \rho_{i-1}\left(-\mathrm{d}\epsilon_{i-1,i-1}^{(k)} + \mathrm{d}\epsilon_{i,i-1}^{(k)}\right)\right)\\
&+ \left(\mathrm{e}^{\gamma_i(x-x_{i-1})} - \mathrm{e}^{-\gamma_i(x-x_{i-1})}\right)\left(\frac{\epsilon_{i,i}^{(k)} + \epsilon_{i+1,i}^{(k)}}{2} + \rho_i\left(-\mathrm{d}\epsilon_{i,i}^{(k)} + \mathrm{d}\epsilon_{i+1,i}^{(k)}\right)\right)\Bigg]
\end{aligned} \tag{9}
$$

and

$$\epsilon_p^{(k+1)}(x) = \frac{\mathrm{e}^{\gamma_p(x_p-x)} - \mathrm{e}^{-\gamma_p(x_p-x)}}{\mathrm{e}^{\gamma_p\ell_p} - \mathrm{e}^{-\gamma_p\ell_p}}\left(\frac{\epsilon_{p-1,p-1}^{(k)} + \epsilon_{p,p-1}^{(k)}}{2} + \rho_{p-1}\left(-\mathrm{d}\epsilon_{p-1,p-1}^{(k)} + \mathrm{d}\epsilon_{p,p-1}^{(k)}\right)\right). \tag{10}$$

Differentiating (8)–(10) we get the following expressions for the derivatives at the interface points:

$$
\begin{aligned}
\mathrm{d}\epsilon_{1,1}^{(k+1)} &= \frac{(\mathrm{e}^{\gamma_1\ell_1} + \mathrm{e}^{-\gamma_1\ell_1})\gamma_1}{\mathrm{e}^{\gamma_1\ell_1} - \mathrm{e}^{-\gamma_1\ell_1}}\left(\frac{\epsilon_{1,1}^{(k)} + \epsilon_{2,1}^{(k)}}{2} + \rho_1\left(-\mathrm{d}\epsilon_{1,1}^{(k)} + \mathrm{d}\epsilon_{2,1}^{(k)}\right)\right),\\
\mathrm{d}\epsilon_{i,i-1}^{(k+1)} &= -\frac{(\mathrm{e}^{\gamma_i\ell_i} + \mathrm{e}^{-\gamma_i\ell_i})\gamma_i}{\mathrm{e}^{\gamma_i\ell_i} - \mathrm{e}^{-\gamma_i\ell_i}}\left(\frac{\epsilon_{i-1,i-1}^{(k)} + \epsilon_{i,i-1}^{(k)}}{2} + \rho_{i-1}\left(-\mathrm{d}\epsilon_{i-1,i-1}^{(k)} + \mathrm{d}\epsilon_{i,i-1}^{(k)}\right)\right)\\
&\quad + \frac{2\gamma_i}{\mathrm{e}^{\gamma_i\ell_i} - \mathrm{e}^{-\gamma_i\ell_i}}\left(\frac{\epsilon_{i,i}^{(k)} + \epsilon_{i+1,i}^{(k)}}{2} + \rho_i\left(-\mathrm{d}\epsilon_{i,i}^{(k)} + \mathrm{d}\epsilon_{i+1,i}^{(k)}\right)\right), \quad i = 2, \ldots, p-1
\end{aligned}
$$

$$\begin{aligned}
\mathrm{d}\epsilon_{i,i}^{(k+1)} &= \frac{2\gamma_i}{\mathrm{e}^{\gamma_i\ell_i}-\mathrm{e}^{-\gamma_i\ell_i}}\left(\frac{\epsilon_{i-1,i-1}^{(k)}+\epsilon_{i,i-1}^{(k)}}{2}+\rho_{i-1}\left(-\mathrm{d}\epsilon_{i-1,i-1}^{(k)}+\mathrm{d}\epsilon_{i,i-1}^{(k)}\right)\right)\\
&\quad+\frac{(\mathrm{e}^{\gamma_i\ell_i}+\mathrm{e}^{-\gamma_i\ell_i})\gamma_i}{\mathrm{e}^{\gamma_i\ell_i}-\mathrm{e}^{-\gamma_i\ell_i}}\left(\frac{\epsilon_{i,i}^{(k)}+\epsilon_{i+1,i}^{(k)}}{2}+\rho_i\left(-\mathrm{d}\epsilon_{i,i}^{(k)}+\mathrm{d}\epsilon_{i+1,i}^{(k)}\right)\right),\quad i=2,\ldots,p-1\\
\mathrm{d}\epsilon_{p,p-1}^{(k+1)} &= -\frac{(\mathrm{e}^{\gamma_p\ell_p}+\mathrm{e}^{-\gamma_p\ell_p})\gamma_p}{\mathrm{e}^{\gamma_p\ell_p}-\mathrm{e}^{-\gamma_p\ell_p}}\left(\frac{\epsilon_{p-1,p-1}^{(k)}+\epsilon_{p,p-1}^{(k)}}{2}+\rho_{p-1}\left(-\mathrm{d}\epsilon_{p-1,p-1}^{(k)}+\mathrm{d}\epsilon_{p,p-1}^{(k)}\right)\right).
\end{aligned}$$

For simplicity, our analysis is carried out only for $p=3$, but it seems that it can be extended for $p>3$ in a way similar to the one found in [12].

We then define the error vector $\underline{\epsilon}^{(k)}$ by ordering the individual errors and their derivatives on the interface points, for $k=0,1,2,\ldots$, as follows

$$\underline{\epsilon}^{(k)} \equiv \left[\epsilon_{1,1}^{(k)},\epsilon_{2,1}^{(k)},\epsilon_{2,2}^{(k)},\epsilon_{3,2}^{(k)},\mathrm{d}\epsilon_{1,1}^{(k)},\mathrm{d}\epsilon_{2,1}^{(k)},\mathrm{d}\epsilon_{2,2}^{(k)},\mathrm{d}\epsilon_{3,2}^{(k)}\right]^{\mathrm{T}}$$

and we then combine the above error expressions into the following recurrence relation between the errors involved in two successive iterations.

$$\underline{\epsilon}^{(k+1)} = M\underline{\epsilon}^{(k)},\quad k=0,1,\ldots, \tag{11}$$

where the iteration matrix $M\in\mathbb{R}^{8\times 8}$ has the form

$$M=\begin{bmatrix}
1/2 & 1/2 & 0 & 0 & -\rho_1 & \rho_1 & 0 & 0\\
1/2 & 1/2 & 0 & 0 & -\rho_1 & \rho_1 & 0 & 0\\
0 & 0 & 1/2 & 1/2 & 0 & 0 & -\rho_2 & \rho_2\\
0 & 0 & 1/2 & 1/2 & 0 & 0 & -\rho_2 & \rho_2\\
A_1\gamma_1/2 & A_1\gamma_1/2 & 0 & 0 & -\rho_1A_1\gamma_1 & \rho_1A_1\gamma_1 & 0 & 0\\
-A_2\gamma_2/2 & -A_2\gamma_2/2 & B_2\gamma_2/2 & B_2\gamma_2/2 & \rho_1A_2\gamma_2 & -\rho_1A_2\gamma_2 & -\rho_2B_2\gamma_2 & \rho_2B_2\gamma_2\\
-B_2\gamma_2/2 & -B_2\gamma_2/2 & A_2\gamma_2/2 & A_2\gamma_2/2 & \rho_1B_2\gamma_2 & -\rho_1B_2\gamma_2 & -\rho_2A_2\gamma_2 & \rho_2A_2\gamma_2\\
0 & 0 & -A_3\gamma_3/2 & -A_3\gamma_3/2 & 0 & 0 & \rho_2A_3\gamma_3 & -\rho_2A_3\gamma_3
\end{bmatrix}, \tag{12}$$

with $A_i=\tanh^{-1}(\gamma_i\ell_i)$ and $B_i=\frac{1}{\sinh(\gamma_i\ell_i)}$ for $i=1,2$.

The following lemma proves that the above given iteration matrix M has the same spectral radius with a simpler matrix of reduced size 2×2.

Lemma 2. *The nonzero eigenvalues of matrix M in (12) are equal to the nonzero eigenvalues of matrix $\tilde{M}$, where*

$$\tilde{M}=\begin{bmatrix}1-\rho_1(\gamma_1A_1+\gamma_2A_2) & \rho_2\gamma_2B_2\\ \rho_1\gamma_2B_2 & 1-\rho_2(\gamma_2A_2+\gamma_3A_3)\end{bmatrix}. \tag{13}$$

Proof. Using basic properties of the determinants we obtain the following equalities:

$$\begin{aligned}
&\det(M-\lambda I_8)\\
&=\det\begin{bmatrix}
-\lambda & 0 & 0 & 0 & 0 & 0 & 0 & 0\\
1/2 & 1-\lambda & 0 & 0 & -\rho_1 & \rho_1 & 0 & 0\\
0 & 0 & -\lambda & 0 & 0 & 0 & 0 & 0\\
0 & 0 & 1/2 & 1-\lambda & 0 & 0 & -\rho_2 & \rho_2\\
A_1\gamma_1/2 & A_1\gamma_1 & 0 & 0 & -\rho_1A_1\gamma_1-\lambda & \rho_1A_1\gamma_1 & 0 & 0\\
-A_2\gamma_2/2 & -A_2\gamma_2 & B_2\gamma_2/2 & B_2\gamma_2 & \rho_1A_2\gamma_2 & -\rho_1A_2\gamma_2-\lambda & -\rho_2B_2\gamma_2 & \rho_2B_2\gamma_2\\
-B_2\gamma_2/2 & -B_2\gamma_2 & A_2\gamma_2/2 & A_2\gamma_2 & \rho_1B_2\gamma_2 & -\rho_1B_2\gamma_2 & -\rho_2A_2\gamma_2-\lambda & \rho_2A_2\gamma_2\\
0 & 0 & -A_3\gamma_3/2 & -A_3\gamma_3 & 0 & 0 & \rho_2A_3\gamma_3 & -\rho_2A_3\gamma_3-\lambda
\end{bmatrix}\\
&=\lambda^2\det\begin{bmatrix}
1-\lambda & 0 & -\rho_1 & \rho_1 & 0 & 0\\
0 & 1-\lambda & 0 & 0 & -\rho_2 & \rho_2\\
A_1\gamma_1 & 0 & -\rho_1A_1\gamma_1-\lambda & \rho_1A_1\gamma_1 & 0 & 0\\
-A_2\gamma_2 & A_2\gamma_2 & \rho_1A_2\gamma_2 & -\rho_1A_2\gamma_2-\lambda & -\rho_2B_2\gamma_2 & \rho_2B_2\gamma_2\\
-B_2\gamma_2 & B_2\gamma_2 & \rho_1B_2\gamma_2 & -\rho_1B_2\gamma_2 & -\rho_2A_2\gamma_2-\lambda & \rho_2A_2\gamma_2\\
0 & -A_3\gamma_3 & 0 & 0 & \rho_2A_3\gamma_3 & -\rho_2A_3\gamma_3-\lambda
\end{bmatrix}\\
&=\lambda^4\det\begin{bmatrix}
-\rho_1A_1\gamma_1-\lambda+1 & \rho_1A_1\gamma_1-1 & 0 & 0\\
\rho_1A_2\gamma_2 & -\rho_1A_2\gamma_2-\lambda & -\rho_2B_2\gamma_2 & \rho_2B_2\gamma_2\\
\rho_1B_2\gamma_2 & -\rho_1B_2\gamma_2 & -\rho_2A_2\gamma_2-\lambda+1 & \rho_2A_2\gamma_2-1\\
0 & 0 & \rho_2A_3\gamma_3 & -\rho_2A_3\gamma_3-\lambda
\end{bmatrix}
\end{aligned}$$

$$= \lambda^4 \det \begin{bmatrix} -\rho_1(A_1\gamma_1 + A_2\gamma_2) - \lambda + 1 & 0 & \rho_2 B_2\gamma_2 & 0 \\ \rho_1 A_2\gamma_2 & -\lambda & -\rho_2 B_2\gamma_2 & 0 \\ \rho_1 B_2\gamma_2 & 0 & -\rho_2(A_2\gamma_2 + A_3\gamma_3) - \lambda + 1 & 0 \\ 0 & 0 & \rho_2 A_3\gamma_3 & -\lambda \end{bmatrix}$$

$$= \lambda^6 \det(\tilde{M} - \lambda I_2). \quad \square$$

We next give our main convergence result.

Theorem 3. *Consider a non-overlapping decomposition of Ω into three subdomains Ω_i of length ℓ_i, $i = 1, 2, 3$ and the following model problem*

$$-\frac{\mathrm{d}^2 u}{\mathrm{d}x^2} + \gamma^2 u = f \quad \text{in } \Omega, \qquad u = u^b \quad \text{on } \partial\Omega. \tag{14}$$

*The **GEO** interface relaxation method converges to the solution of the above problem, if and only if its relaxation parameters satisfy the following inequalities:*

$$0 < \rho_1 < \frac{2}{C_1}, \qquad 0 < \rho_2 < 2\frac{2 - \rho_1 C_1}{2C_2 - \rho_1(C_1 C_2 - \gamma_2^2 B_2^2)}, \tag{15}$$

where $C_i = \gamma_i A_i + \gamma_{i+1} A_{i+1}$, $i = 1, 2$, and where γ_i is the restriction of γ in Ω_i.

Proof. For the convergence of the method, we will show that the spectral radius of the iteration matrix is less than one. According to the previous lemma, this is equivalent to proving that the spectral radius of $\tilde{M}$ is less than one. Setting $D_i = 1 - \rho_i C_i$, $i = 1, 2$, we have the following characteristic polynomial

$$\det(\tilde{M} - \lambda I_2) = 0 \Leftrightarrow \lambda^2 - \lambda(D_1 + D_2) + D_1 D_2 - \rho_1\rho_2\gamma_2^2 B_2^2 = 0,$$

whose roots are

$$\lambda_{1,2} = \frac{D_1 + D_2 \pm \sqrt{(D_1 - D_2)^2 + 4\rho_1\rho_2(\gamma_2 B_2)^2}}{2}. \tag{16}$$

To determine the region of convergence, we simply impose the inequality $|\lambda_{1,2}| < 1$ and solve with respect to ρ_1, ρ_2. We note that the same conditions would have been obtained if we had applied the Schur–Cohn algorithm [3].

Since $\rho_1, \rho_2 > 0$, it is clear that the quantity under the square root in (16) is positive and thus $\lambda_1, \lambda_2 \in \mathbb{R}$. Furthermore, it is easy to see that

$$\lambda_{1,2} < 1, \quad \forall \rho_i, \gamma_i, \ell_i, i = 1, 2, 3.$$

To prove this it is equivalent to proving that

$$-\rho_1(\gamma_1 A_1 + \gamma_2 A_2) - \rho_2(\gamma_2 A_2 + \gamma_3 A_3) \pm \sqrt{\rho_1(\gamma_1 A_1 + \gamma_2 A_2) - \rho_2(\gamma_2 A_2 + \gamma_3 A_3) + 4\rho_1\rho_2(\gamma_2 B_2)^2} < 0.$$

The above is obviously true for the negative case while for the positive case we easily obtain the following equivalent inequalities

$$4\rho_1\rho_2(\gamma_2 B_2)^2 < 4\rho_1\rho_2(\gamma_1 A_1 + \gamma_2 A_2)(\gamma_2 A_2 + \gamma_3 A_3)$$

$$\Leftrightarrow \gamma_1\gamma_2 A_1 A_2 + \gamma_2\gamma_3 A_2 A_3 + \gamma_1\gamma_3 A_1 A_3 + \gamma_2^2 \left(\frac{\cosh^2(\gamma_2\ell_2) - 1}{\sinh^2(\gamma_2\ell_2)}\right) > 0$$

and realize that the latter always holds since $\frac{\cosh^2(\gamma_2\ell_2)-1}{\sinh^2(\gamma_2\ell_2)}$, γ_i, ℓ_i and $A_i = 1, 2, 3$ are all positive. Also

$$\lambda_{1,2} > -1 \Leftrightarrow -4 + \rho_1 C_1 + \rho_2 C_2 < \pm\sqrt{(C_1 - C_2)^2 + 4\rho_1\rho_2(\gamma_2 B_2)^2}$$

which forces $-4 + \rho_1 C_1 + \rho_2 C_2 < 0$. This holds if

$$(\rho_1, \rho_2) \in R_1 = \left\{ (x, y) \in \mathbb{R}^2 \,\middle|\, x < \frac{4}{C_1},\ y < \frac{4 - \rho_1 C_1}{C_2} \right\}. \tag{17}$$

For the ρ_i, $i = 1, 2$, to be in the above set, it is sufficient to just solve the inequality

$$-4 + \rho_1 C_1 + \rho_2 C_2 < -\sqrt{(C_1 - C_2)^2 + 4\rho_1\rho_2(\gamma_2 B_2)^2}$$

or equivalently the following inequality

$$4 - 2\rho_1 C_1 - 2\rho_2 C_2 + \rho_1\rho_2(C_1 C_2 - \gamma_2^2 B_2^2) > 0.$$

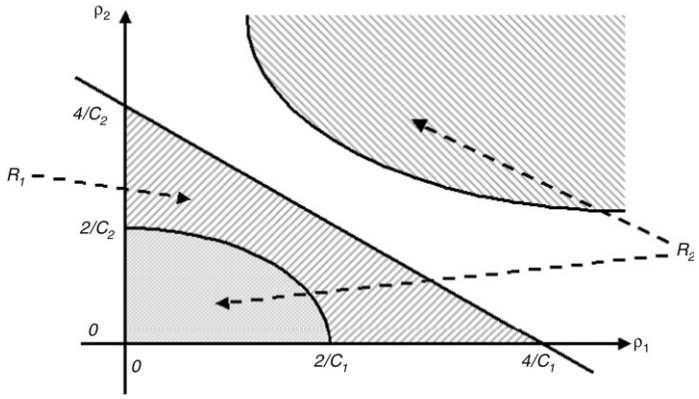

Fig. 2. Region of convergence for the relaxation parameters of the **GEO** method.

This is true in the areas enclosed by the two hyperbolas shown in Fig. 2, i.e.,

$$(\rho_1, \rho_2) \in R_2 = \left\{ (x, y) \in \mathbb{R}^2 \middle| \; x < \frac{2}{C_1}, \; y < 2\frac{2 - xC_1}{2C_2 - x(C_1C_2 - \gamma_2^2 B_2^2)} \right\}. \tag{18}$$

We conclude the proof of this theorem by taking the intersections of the regions in (17) and (18) (see Fig. 2) and the fact that $\rho_i > 0, i = 1, 2$. □

In an effort to elucidate the convergence characteristics of the **GEO** method we consider simpler model problems by restricting the values of γ and p in the above theorem and we easily obtain the following corollaries.

Corollary 4. *If we replace in (14) in Theorem 3 the Helmholtz operator with the Laplacian (i.e., set $\gamma^2 = 0$), and consider the same decomposition, the region of convergence of the **GEO** method becomes*

$$0 < \rho_1 < \frac{2}{\Gamma_1}, \qquad 0 < \rho_2 < 2\frac{2 - \rho_1\Gamma_1}{2\Gamma_2 - \rho_1(\Gamma_1\Gamma_2 - 1/\ell_2^2)},$$

where $\Gamma_i = \frac{\ell_i + \ell_{i+1}}{\ell_i \ell_{i+1}}, i = 1, 2$.

Proof. As can be easily verified, the solution of the differential equation problem

$$-\frac{\mathrm{d}^2 u}{\mathrm{d}x^2} = 0, \quad x \in (a, b), \qquad u(a) = u_1, \qquad u(b) = u_2$$

is given by $u(x) = \frac{u_1(b-x)}{b-a} + \frac{u_2(x-a)}{b-a}$. Using this to obtain, as in Theorem 3, the recurrence relation between the errors at subsequent iteration steps and following the same procedure as in Theorem 3 and in Lemma 2, we conclude the region of convergence for the two relaxation parameters. □

Corollary 5. *Assume that we have a two subdomain partition of the domain Ω with homogeneous boundary conditions on its boundary. Then*

- *For the Laplace operator:*
  - *The **GEO** method converges if and only if $0 < \rho_1 < 2\frac{\ell_1\ell_2}{\ell_1+\ell_2}$.*
  - *The optimum value of the **GEO** relaxation parameter is*
    $$\rho_1 = \frac{\ell_1\ell_2}{\ell_1 + \ell_2}$$
    which makes the method to converge immediately.
- *For the Helmholtz operator:*
  - *The **GEO** method converges if and only if $0 < \rho_1 < 2/(\gamma_1 \tanh^{-1}(\gamma_1\ell_1) + \gamma_2 \tanh^{-1}(\gamma_2\ell_2))$.*
  - *The optimum value of the **GEO** relaxation parameter is*
    $$\rho_1 = 1/(\gamma_1 \tanh^{-1}(\gamma_1\ell_1) + \gamma_2 \tanh^{-1}(\gamma_2\ell_2))$$
    which makes the method to converge immediately.

Proof. The proof follows (and in fact is much simpler) the proofs of Theorem 3 and Corollary 4. □

Although the theory in the previous corollary indicates that the convergence is immediate (in 1 iteration), it can be shown, [15], that this is not the case in the numerical experiments mainly due to the particular block structure of the Jordan form of the iteration matrices which for p subdomains may require from 1 to $2(p-1)$ iteration steps (instead of one) for convergence.

4. Convergence analysis at discrete level

In this section we give the analysis on the discrete (Linear Algebra) level. We consider the Laplace equation and split Ω into the three subdomains Ω_i, $i = 1, 2, 3$. We denote the interface points as I_1 and I_2 and we discretize each subdomain using $n_i + 1$, $i = 1, 2, 3$, uniformly distributed points. To discretize the Laplace operator we use the standard 5-point star scheme. Denoting by $I_0 = a$, $I_3 = b$ and $h_i = \frac{I_i - I_{i-1}}{n_i}$, $i = 1, 2, 3$, we define the discretization points in Ω_i as $x_{j_i}^{(i)} = I_{i-1} + h_i j_i$ with $j_i = 0, \ldots, n_i$, for $i = 1, 2, 3$. For an approximation of the derivative from the left side on the interface points we use Taylor series expansion to obtain that

$$\left.\frac{\mathrm{d}u}{\mathrm{d}x}\right|_{x=x^\star} = \frac{1}{h}\left(\frac{3}{2}u(x^\star) - 2u(x^\star - h) + \frac{1}{2}u(x^\star - 2h)\right) + O(h^2).$$

Taking into account the points from the right side, we similarly have

$$\left.\frac{\mathrm{d}u}{\mathrm{d}x}\right|_{x=x^\star} = \frac{1}{h}\left(-\frac{3}{2}u(x^\star) + 2u(x^\star + h) - \frac{1}{2}u(x^\star + 2h)\right) + O(h^2).$$

Let us now denote with u_{i,h_i} the discrete solution of the original problem in subdomain Ω_i, by $\epsilon_{j_i}^{(i,k)} \equiv u_{i,h_i}^{(k)}(x_{j_i}^{(i)}) - u_{i,h_i}(x_{j_i}^{(i)})$, the error on point $x_{j_i}^{(i)}$ at the kth iteration, and define the iteration error vectors as

$$\underline{\epsilon}^{(k)} \equiv \left[\epsilon_1^{(1,k)}, \epsilon_2^{(1,k)}, \ldots, \epsilon_{n_1}^{(1,k)}, \epsilon_0^{(2,k)}, \epsilon_1^{(2,k)}, \ldots, \epsilon_{n_2}^{(2,k)}, \epsilon_0^{(3,k)}, \epsilon_1^{(3,k)}, \ldots, \epsilon_{n_3-1}^{(3,k)}\right]^{\mathrm{T}}.$$

As in the previous section we easily derive the following recurrence relation between the error vectors on two successive iterants.

$$\underline{\epsilon}^{(k+1)} = M\underline{\epsilon}^{(k)}, \quad k = 0, 1, \ldots, \text{ with } M = T^{-1}N \tag{19}$$

where

$$T = \begin{bmatrix} T_2^{(n_1-1)} & 0 & 0 & 0 & 0 \\ 0 & I_2 & 0 & 0 & 0 \\ 0 & 0 & T_2^{(n_2-1)} & 0 & 0 \\ 0 & 0 & 0 & I_2 & 0 \\ 0 & 0 & 0 & 0 & T_2^{(n_3-1)} \end{bmatrix},$$

$$N = \begin{bmatrix} 0_{n_1-2,n_1-3} & 0 & 0 & 0 & 0 \\ 0 & N_1 & 0 & 0 & 0 \\ 0 & 0 & 0_{n_2-3,n_2-5} & 0 & 0 \\ 0 & 0 & 0 & N_2 & 0 \\ 0 & 0 & 0 & 0 & 0_{n_3-2,n_3-3} \end{bmatrix},$$

$T_2^{(n)} \equiv \mathrm{tridiag}\{-1, 2, -1\} \in \mathrm{R}^{n\times n}$, I_2 is the 2×2 identity matrix, $N_i \in \mathbb{R}^{4\times 6}$, $i = 1, 2$, while $0_{n,m} \in \mathbb{R}^{n\times m}$ has all its elements equal to 0 and $N_i = [1\ 1\ 1\ 1\ 1\ 1]^{\mathrm{T}}[a_i\ b_i\ c_i\ d_i\ e_i\ f_i]$, with $a_i = -\rho_i/(2h_i)$, $b_i = 2\rho_i/h_i$, $c_i = 1/2 - 3\rho_i/(2h_i)$, $d_i = 1/2 - 3\rho_i/(2h_{i+1})$, $e_i = 2\rho_i/h_{i+1}$, $f_i = -\rho_i/(2h_{i+1})$, $i = 1, 2$.

Lemma 6. *The first and the last columns of the inverse matrix of $T_2^{(n)}$ are equal to the following vectors correspondingly,*

$$[1/n, \ldots, (n-1)/n]^{\mathrm{T}}, \qquad [(n-1)/n, \ldots, 1/n]^{\mathrm{T}}.$$

Proof. The above formulas for the vectors are well known. They can be readily derived using elementary analysis of difference equations. □

Lemma 7. *The nonzero eigenvalues of matrix M in (19) are equal to the nonzero eigenvalues of the matrix*

$$\tilde{M} = \begin{bmatrix} 1 - \rho_1\Gamma_1 & \frac{\rho_1}{h_2} & 0 & 0 \\ 0 & 0 & \frac{\rho_2}{\ell_2} & \frac{1-\rho_2\Gamma_2}{n_2} \\ \frac{1-\rho_1\Gamma_1}{n_2} & \frac{\rho_1}{\ell_2} & 0 & 0 \\ 0 & 0 & \frac{\rho_2}{h_2} & 1 - \rho_2\Gamma_2 \end{bmatrix}, \tag{20}$$

where the Γ_i, $i = 1, 2$, are given in Corollary 4.

Proof. Using properties of the determinant, we can see that,

$$\det(M-\lambda I_{n_1+n_2+n_3+1}) = \lambda^{n_1+n_2+n_3-11}\det\begin{bmatrix} N_{1,1} & N_{1,2} \\ N_{2,1} & N_{2,2}\end{bmatrix},$$

where

$$N_{i,i} = \left[g_i\ \widetilde{h}_i\ 1\ 1\ \widetilde{h}_{i+1}\ g_{i+1}\right]^{\mathrm{T}}[a_i\ b_i\ c_i\ d_i\ e_i\ f_i] - \lambda I_6, \quad i = 1, 2,$$

with $g_i = \frac{n_i-2}{n_i}$, $\widetilde{h}_i = \frac{n_i-1}{n_i}$ and $N_{1,2} = \frac{1}{n_2}[0\,0\,0\,0\,1\,2]^{\mathrm{T}}[a_i\ b_i\ c_i\ d_i\ e_i\ f_i]$ and $N_{2,1} = \frac{1}{n_2}[2\,1\,0\,0\,0\,0]^{\mathrm{T}}[a_i\ b_i\ c_i\ d_i\ e_i\ f_i]$. Also,

$$\det(M-\lambda I_{n_1+n_2+n_3+1}) = \lambda^{n_1+n_2+n_3-7}$$

$$\times\ \det\begin{bmatrix}
\frac{1}{2}-\frac{\rho_1}{\ell_1} & \frac{1}{2}-\frac{\rho_1}{\ell_2} & e_1 & f_1 & 0 & 0 & 0 & 0 \\
\frac{1}{2}-\frac{\rho_1}{\ell_1} & \frac{1}{2}-\frac{\rho_1}{\ell_2} & e_1 & f_1 & 0 & 0 & 0 & 0 \\
0 & 0 & 0 & 0 & \frac{a_2}{n_2} & \frac{b_2}{n_2} & \frac{1}{2n_2}-\frac{\rho_2}{n_2\ell_2} & \frac{1}{2n_2}-\frac{\rho_2}{n_2\ell_3} \\
0 & 0 & 0 & 0 & \frac{2a_2}{n_2} & \frac{2b_2}{n_2} & \frac{1}{n_2}-\frac{2\rho_2}{n_2\ell_2} & \frac{1}{n_2}-\frac{2\rho_2}{2\ell_3} \\
\frac{1}{n_2}-\frac{2\rho_1}{\ell_1 n_2} & \frac{1}{n_2}-\frac{2\rho_1}{\ell_2 n_2} & \frac{2e_1}{n_2} & \frac{2f_1}{n_2} & 0 & 0 & 0 & 0 \\
\frac{1}{2n_2}-\frac{\rho_1}{\ell_1 n_2} & \frac{1}{2n_2}-\frac{\rho_1}{\ell_2 n_2} & \frac{e_1}{n_2} & \frac{f_1}{n_2} & 0 & 0 & 0 & 0 \\
0 & 0 & 0 & 0 & a_2 & b_2 & \frac{1}{2}-\frac{\rho_2}{\ell_2} & \frac{1}{2}-\frac{\rho_2}{\ell_3} \\
0 & 0 & 0 & 0 & a_2 & b_2 & \frac{1}{2}-\frac{\rho_2}{\ell_2} & \frac{1}{2}-\frac{\rho_2}{\ell_3}
\end{bmatrix} - \lambda I_8$$

$$= \lambda^{n_1+n_2+n_3-5}\det\begin{bmatrix}
1-\rho_1\Gamma_1 & f_1 & 0 & \frac{\rho_1}{h_2} & 0 & 0 \\
0 & 0 & a_2/n_2 & 0 & \frac{\rho_2}{\ell_2} & \frac{1-\rho_2\Gamma_2}{n_2} \\
0 & 0 & 0 & 0 & 0 & 0 \\
0 & 0 & 0 & 0 & 0 & 0 \\
\frac{1-\rho_1\Gamma_1}{n_2} & f_1/n_2 & 0 & \frac{\rho_1}{\ell_2} & 0 & 0 \\
0 & 0 & 0 & a_2 & \frac{\rho_2}{h_2} & 1-\rho_2\Gamma_2
\end{bmatrix} - \lambda I_6$$

$$= \lambda^{n_1+n_2+n_3-3}\det(\tilde{M}-\lambda I_4). \quad \square$$

Theorem 8. *Consider the Laplace equation, Dirichlet boundary conditions and a non-overlapping decomposition of Ω into three subdomains Ω_i of lengths ℓ_i, $i = 1, 2, 3$. Consider also the discretization described at the beginning of the section. The convergence of **GEO** interface relaxation method is independent of h_i, $i = 1, 2, 3$, and the region of convergence is the same as in Corollary 4.*

Proof. According to the previous lemma, it is sufficient to prove that the spectral radius of $\tilde{M}$ is less than one. But

$$\det(\tilde{M}-\lambda I_4) = \det\begin{bmatrix}
1-\rho_1\Gamma_1-\lambda & \frac{\rho_1}{h_2} & 0 & 0 \\
0 & -\lambda & 0 & \lambda/n_2 \\
\lambda/n_2 & 0 & -\lambda & 0 \\
0 & 0 & \frac{\rho_2}{h_2} & 1-\rho_2\Gamma_2-\lambda
\end{bmatrix}$$

$$= (1-\rho_1\Gamma_1-\lambda)\det\begin{bmatrix}
\lambda & 0 & -\lambda/n_2 \\
0 & -\lambda & 0 \\
0 & \frac{\rho_2}{h_2} & 1-\rho_2\Gamma_2-\lambda
\end{bmatrix} + \frac{\lambda}{n_2}\det\begin{bmatrix}
\frac{\rho_1}{h_2} & 0 & 0 \\
-\lambda & 0 & \lambda/n_2 \\
0 & \frac{\rho_2}{h_2} & 1-\rho_2\Gamma_2-\lambda
\end{bmatrix} = 0.$$

Therefore, to compute the nonzero eigenvalues we have to solve the equation

$$(1-\rho_1\Gamma_1-\lambda)(1-\rho_2\Gamma_2-\lambda) - \frac{\rho_1}{h_2 n_2}\frac{\rho_2}{h_2 n_2} = 0$$

which is equivalent to

$$\lambda^2 - \lambda(2 - \rho_1\Gamma_1 - \rho_2\Gamma_2) + (1 - \rho_1\Gamma_1)(1 - \rho_2\Gamma_2) - \frac{\rho_1\rho_2}{\ell_2^2} = 0.$$

It is clear that the coefficients of the above polynomial are independent of h_i and n_i, and depend only on the decomposition of Ω. Continuing in the same way as in Theorem 3, we easily conclude the proof. □

It is worth noting that the above theorem proves that $\lim_{k\to\infty} \underline{\epsilon}^{(k+1)} = 0$ which means that $u_{i,h_i}^{(k)} \to u_{i,h_i}$, as $k \to \infty$.

Since $\rho(M) < 1$ there exists a natural norm $|||.|||$ in $\mathrm{R}^{\left(\sum_{i=1}^{3} n_i+1\right)\times\left(\sum_{i=1}^{3} n_i+1\right)}$, such that $c^\star \equiv |||M||| < 1$. Then, if we denote by

$$\begin{aligned}
\underline{u}_{\Delta}^{(k)} \equiv \Big[& u_{1,h_1}^{(k)}(x_1^{(1)}), u_{1,h_1}^{(k)}(x_2^{(1)}), \ldots, u_{1,h_1}^{(k)}(x_{n_1}^{(1)}), u_{2,h_2}^{(k)}(x_0^{(2)}), u_{2,h_2}^{(k)}(x_1^{(2)}), \ldots, u_{2,h_2}^{(k)}(x_{n_2}^{(2)}) \ , \\
& u_{3,h_3}^{(k)}(x_0^{(3)}), u_{3,h_3}^{(k)}(x_1^{(3)}), \ldots, u_{3,h_3}^{(k)}(x_{n_3-1}^{(3)}) \Big]^{\mathrm{T}} , \\
\underline{u}_{\Delta} \equiv \Big[& u_{1,h_1}(x_1^{(1)}), u_{1,h_1}(x_2^{(1)}), \ldots, u_{1,h_1}(x_{n_1}^{(1)}), u_{2,h_2}(x_0^{(2)}), u_{2,h_2}(x_1^{(2)}), \ldots, u_{2,h_2}(x_{n_2}^{(2)}), \\
& u_{3,h_3}(x_0^{(3)}), u_{3,h_3}(x_1^{(3)}), \ldots, u_{3,h_3}(x_{n_3-1}^{(3)}) \Big]^{\mathrm{T}}
\end{aligned}$$

and

$$\underline{u} \equiv \left[u(x_1^{(1)}), u(x_2^{(1)}), \ldots, u(x_{n_1}^{(1)}), u(x_0^{(2)}), u(x_1^{(2)}), \ldots, u(x_{n_2}^{(2)}), u(x_0^{(3)}), u(x_1^{(3)}), \ldots, u(x_{n_3-1}^{(3)}) \right]^{\mathrm{T}}$$

we have that

$$\begin{aligned}
|||\underline{u}_{\Delta}^{(k+1)} - \underline{u}||| &\le |||\underline{\epsilon}^{(k+1)}||| + |||\underline{u}_{\Delta} - \underline{u}||| \le c^* |||\underline{\epsilon}^{(k)}||| + c_\star H^2 \\
&\le \cdots \le (c^\star)^{k+1} |||\epsilon^{(0)}||| + c_\star H^2,
\end{aligned}$$

where $H = \max_{1\le i\le 3}\{h_i\}$. Note that, $c^\star$ is independent of h_i, n_i, $i = 1, 2, 3$ while $c_\star$ depends only on the smoothness of u.

Finally, we would like to present the results for the trivial two-domain case for both Laplace and Helmholtz PDE operators.

Corollary 9. *The region of convergence and the optimum value of the relaxation parameter are as in Section 3 for the two-domain case with the Laplace PDE operator. For the corresponding Helmholtz PDE problem the region of convergence is the interval* $(0, \frac{2}{A^\star + B^\star})$*, while the optimum value is equal to* $(A^\star + B^\star)^{-1}$*, where*

$$A^\star = \frac{1}{2h_1}\left(3 + \frac{\sinh((n_1-2)\theta_1)}{\sinh(n_1\theta_1)} - 4\frac{\sinh((n_1-1)\theta_1)}{\sinh(n_1\theta_1)}\right)$$

and

$$B^\star = \frac{1}{2h_2}\left(3 + \frac{\sinh((n_2-2)\theta_2)}{\sinh(n_2\theta_2)} - 4\frac{\sinh((n_2-1)\theta_2)}{\sinh(n_2\theta_2)}\right)$$

and θ_i *satisfies the equation* $2\cosh(\theta_i) = 2 + \gamma_i^2 h_i^2$, $i = 1, 2$. *In both cases, using the optimum value for the relaxation parameter leads to immediate convergence (in the sense of Corollary 5) to the solution of the initial problem.*

5. Numerical experiments

The purpose of this section is to verify the above given theoretical results (and in particular Theorems 3 and 8) by experimentally examining their validity. The robustness of the proposed method with respect to certain parameters of the differential problems and their decomposition is also examined by means of an elementary sensitivity analysis.

A new problem solving environment based on the general interface relaxation framework and the associated methods already proposed is under way. For this paper we have implemented the **GEO** method for 1- and 2-dimensional problems using MATLAB[1] and we restricted our experiments to partitions in two or three subdomains. Numerical data that are associated with the application of the **GEO** method to decompositions in more than three 1-dimensional subdomains can be found in [11]. These data together with additional numerical experiments for the method **GEO** not presented in this paper, as well as implementations and performance data associated with several other *IR* schemes can also be found in the above-mentioned web page.

[1] All MATLAB files used to produce the numerical data in this section are available at http://mav.inf.uth.gr/r-and-d/software/interface-relaxation.

5.1. One-dimensional boundary value problems

Let us consider the following model problem:

$$Lu \equiv -u''(x) + \gamma^2 u(x) = f(x), \quad x \in (0,1), \qquad u(0) = u^0, \qquad u(1) = u^1, \tag{21}$$

where the right-hand-side function f and the boundary values u^0 and u^1 are selected such that the true solution $u(x)$ is $u(x) = e^{x+4}x(x-1)(x-.7)$. For the coefficient γ^2 several values will be considered. We note that the above problem has been also considered in our preliminary experimental analysis in [11]. Summarizing those experimental findings we mention that by applying the **GEO** scheme to the above problem and other similar 1-dimensional problems one might safely claim that:

- The **GEO** method converges faster than most of the other *IR* schemes for a large class of problems.
- Its rate of convergence is minimally affected by the various parameters involved.
- It usually converges in a rather systematic way.
- Its implementation is rather easy.

These observations are further confirmed and enhanced by the numerical data presented in the rest of this section.

Let us now consider the Boundary Value Problems that are associated with (21) and the corresponding three different configurations (with respect to the values of the coefficient γ_i^2, $i = 1, 2, 3$ and the position of the two interface points x_1 and x_2) as shown below.

BVPA: $x_1 = 1/3, x_2 = 2/3$ and $\gamma_1^2 = \gamma_2^2 = \gamma_3^2 = 4$.
BVPB: $x_1 = 0.2, x_2 = 0.7$ and $\gamma_1^2 = \gamma_2^2 = \gamma_3^2 = 4$.
BVPC: $x_1 = 0.2, x_2 = 0.7$ and $\gamma_1^2 = 2, \gamma_2^2 = 10$ and $\gamma_3^2 = 4$.

Each of the three subdomains is discretized using the second order finite difference scheme with step size h (common to all three subproblems) and uses zero as initial guesses on the interfaces. In Fig. 4 we present the plots of the max norm of the error $u^{(k)} - u$ for the three boundary values problems considered versus the iteration number k. As can be clearly seen ????

In left part of Fig. 3 we present the contour plots of the experimentally estimated number of iterations required to reduce the max norm of the difference of two successive iterants, $\|u^{(k)} - u^{(k-1)}\|_\infty$ ($u^{(k)}$ denotes the computed solution at iteration $k = 1, 2, \ldots$) below 10^{-5} as a function of the two relaxation parameters involved, ρ_1 and ρ_2. The stars in these plots correspond to the experimentally estimated (by systematically varying the values of the relaxation parameters and comparing the corresponding number of iterations required for convergence) optimal values of the relaxation parameters ρ_1 and ρ_2. We mention that for those "optimum" values convergence was achieved in 17, 12 and 10 iterations for BVP A, BVP B and BVP C respectively.

In the plots in the right part of Fig. 3 we present the contours of the theoretically determined upper bound of the spectral radius of the **GEO** method associated with the three BVP configurations described above. Specifically, we plot $\max\{|\lambda_1|, |\lambda_2|\}$ where the λ_i's are those given in Eq. (16). The stars in these plots indicate the case where $\rho_i = \frac{1}{C_i}$, $i = 1, 2$ which seems to be a reasonable choice for "good" values since they zero the centers of the Gerschgorin disks of the matrix in (13) while they keep the spectral radius less than one. For those "good" values λ_{ρ_1,ρ_2} is equal to 0.4063, 0.2404 and 0.1733 for BVP A, BVP B and BVP C respectively.

The perfect matching between the theoretical and the experimental data is clearly depicted. Both the convergence region and the location of the optimum cases are in accordance. We furthermore observe that the variations on the subdomain splitting and the different γ's do not drastically change the region of convergence. It is also seen that when the values of ρ's have at least two correct significant digits then reasonably fast convergence is achieved.

We conclude this subsection by presenting in Fig. 5 the history of convergence for the three boundary value problem configurations considered using $\rho_1 = \rho_2 = 0.14$. Specifically, we plot the max norm of relative successive differences $\frac{\|u^{(k)} - u^{(k-1)}\|_\infty}{\|u^{(k)}\|_\infty}$ versus k. In the plots on the left part of the figure we systematically vary the discretization step of the finite difference used as follows, $h = 0.1/(2^i)$ for $i = 0, 1, 2, 3$. As is apparent, and in fact very much anticipated, the **GEO** method does not depend at all on the parameter associated with the discretization resolution on each subdomain. Finally, from the data shown in the plots on the right part of Fig. 5, we can easily claim that the convergence of the method depends very little on the value of the coefficient γ^2.

5.2. Two-dimensional elliptic partial differential problems

The convergence analysis of the general case (e.g., arbitrary 2-dimensional decompositions) of the **GEO** method for elliptic PDEs is currently under development and will be presented elsewhere. Nevertheless, here we would like to experimentally examine its applicability and its convergence characteristics on simple decompositions. For this let us consider the following elliptic problem:

$$\begin{aligned} Lu(x,y) \equiv -\nabla^2 u(x,y) + \gamma^2 u(x,y) &= f(x,y), \quad (x,y) \in \Omega \\ u(x,y) &= u^b(x,y), \quad (x,y) \in \partial\Omega, \end{aligned} \tag{22}$$

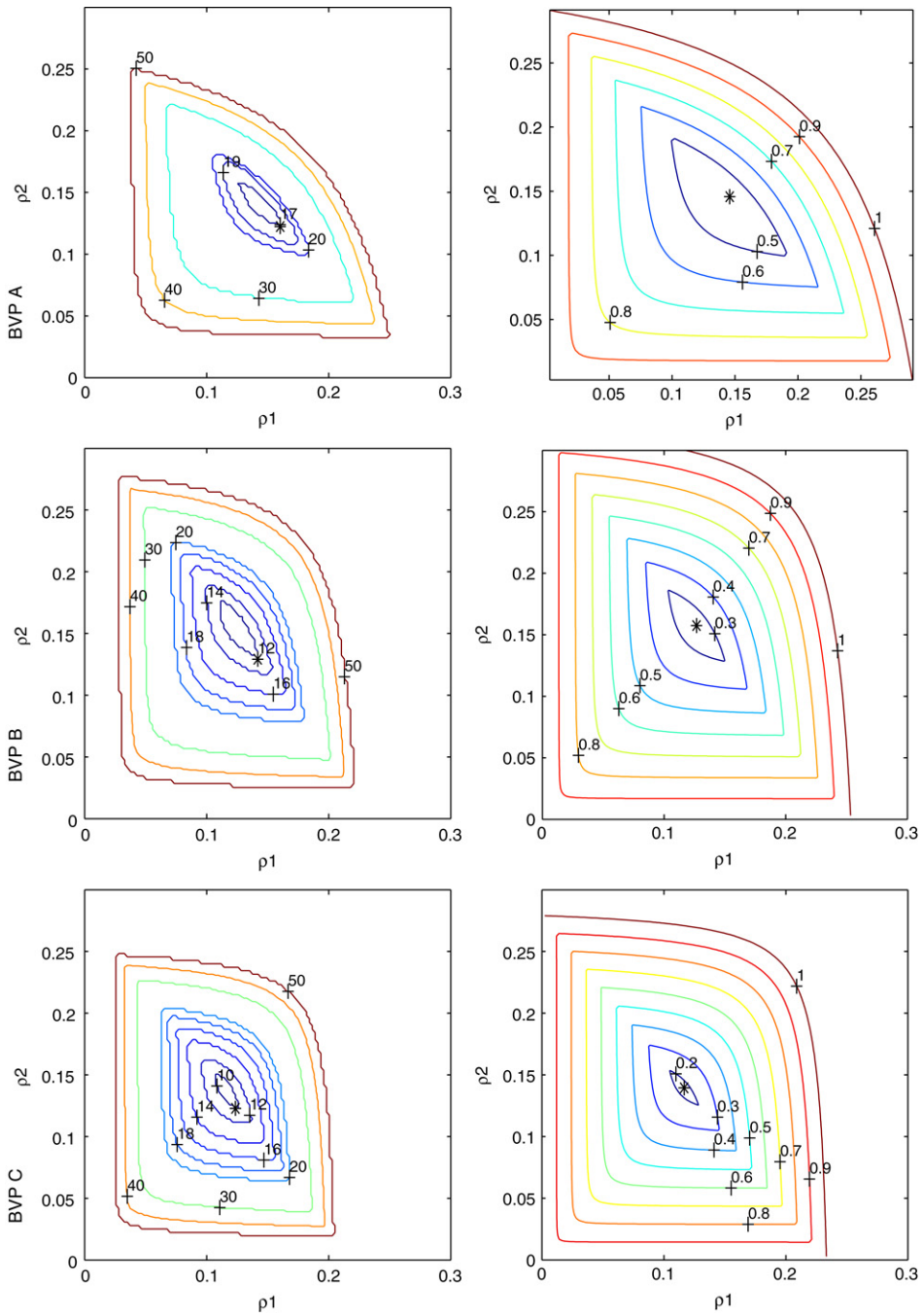

Fig. 3. Contour plots of the number of iterations required for convergence (plots on the left) and of the upper bounds of the spectral radius (plots on the right) with respect to the values of the interface relaxation parameters ρ_1 and ρ_2 for the three boundary value problems.

where the right-hand-side function $f(x, y)$ and the boundary value function $u^b(x, y)$ are selected such that the true solution $u(x, y)$ is

$$u(x, y) = e^{y(x+4)}x(x-1)(x-.7)y(y-.5). \tag{23}$$

We consider two different PDE problems consisting of the differential equation and the boundary conditions given in (22) and the two different domains depicted in Fig. 9. Specifically we denote by PDE A the one whose domain is associated with the plots in the first row of the figure and PDE B the one whose domain is associated with the plots in the second row of the figure. The decomposition of both PDE problems into three subproblems is also defined by the plots in this figure — the two

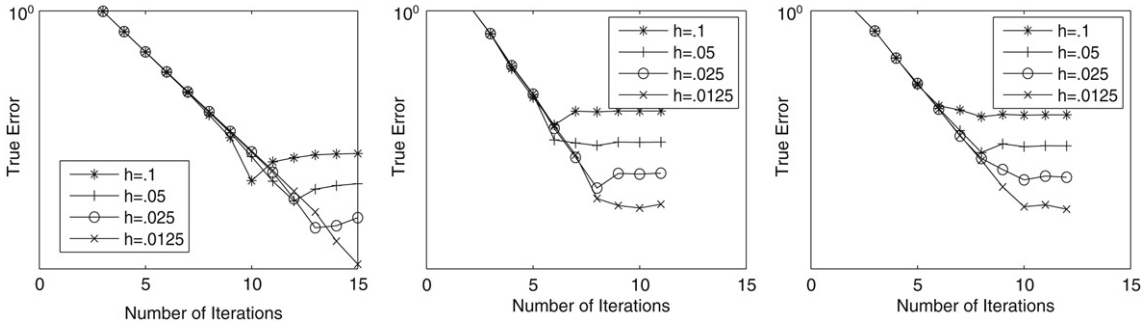

Fig. 4. Plots of max norm of the computed error $\|u^{(k)} - u\|$ versus the iteration number k for BVP A (left), BVP B (middle) and BVP C (right) for four different space discretizations with $h = 0.1/(2^i)$ for $i = 0, 1, 2, 3$.

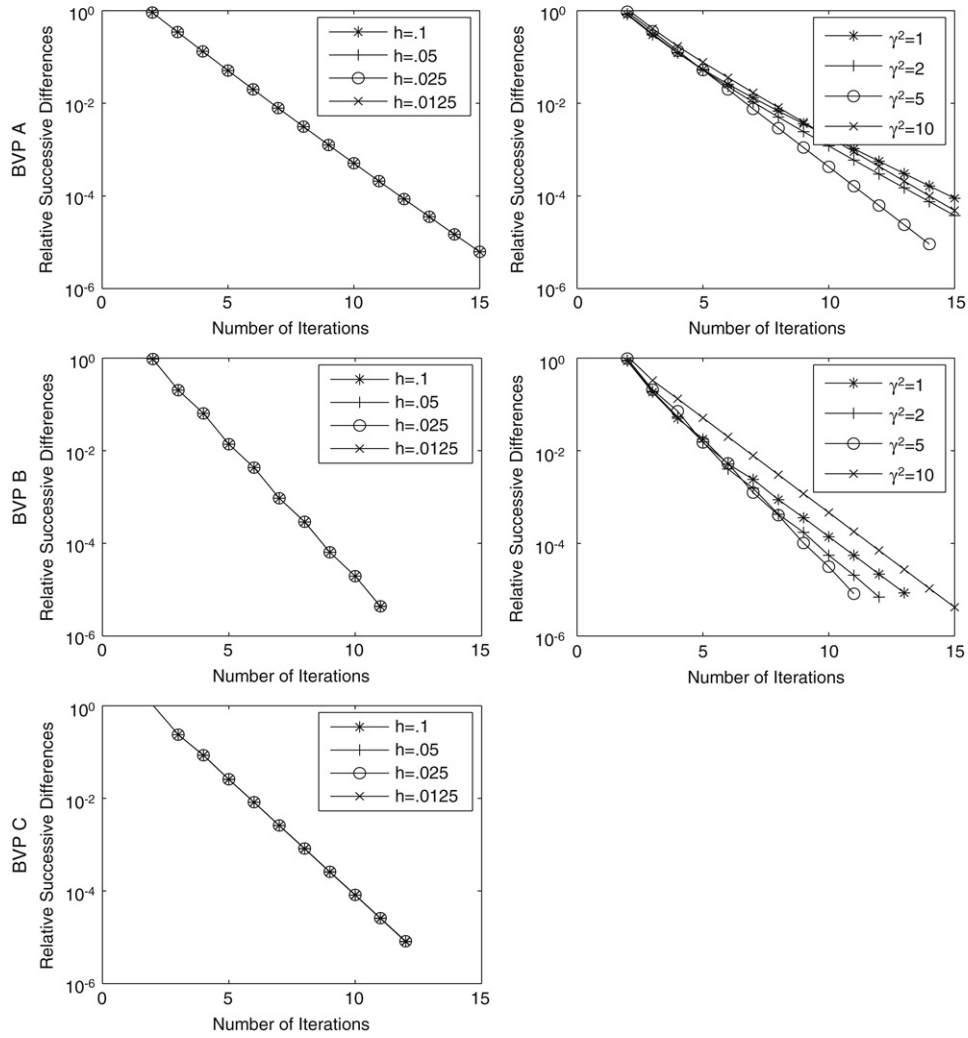

Fig. 5. Plots of max norm of the relative difference of two successive iterants versus the number of iterations for different space discretizations $h = 0.1/(2^i)$ for $i = 0, 1, 2, 3$ (plots on the left) and for different values of the coefficient γ^2 (plots on the right) for the three boundary value problems.

interface points for PDE A are at $x_1 = \frac{1}{3}$ and $x_2 = \frac{2}{3}$ while for PDE B are at $x_1 = \frac{1}{5}$ and $x_2 = \frac{1}{2}$. We use zero as initial guess and unless otherwise explicitly stated we set $\gamma^2 = 2$ and we discretize each subdomain using $h = 0.05$.

Our MATLAB implementation of the **GEO** method used in the following 2-dimensional experiments is quite general allowing us to define the wide variety of problems required for our experimental study and beyond. The MATLAB's

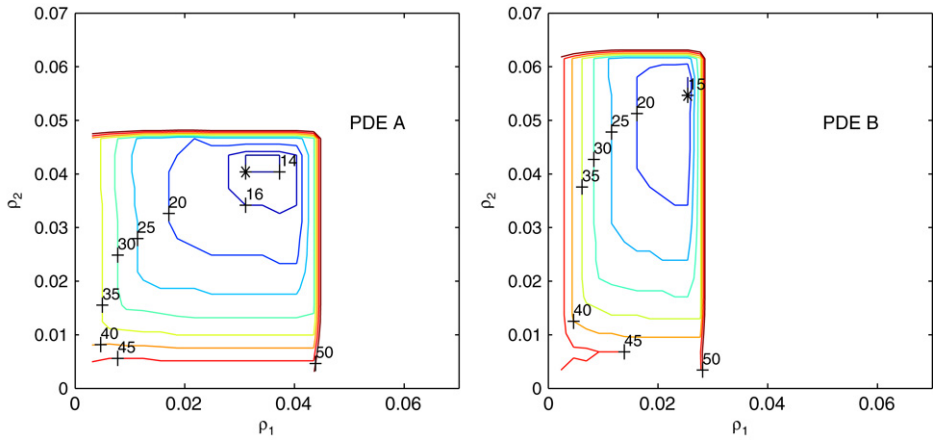

Fig. 6. Contour plots of the number of iterations required for convergence with respect to the values of the interface relaxation parameters ρ_1 and ρ_2 for the two PDE problems.

PDE Toolbox[2] is used to specify the main characteristics of the problem's subdomains (i.e., geometry, PDE operator and boundary/interface conditions). The generated MATLAB files are then used by the main script that realizes the interface relaxation procedure. MATLAB procedures contained in the PDE Toolbox are used to generate and/or refine meshes (triangular elements) for each subdomain, solve the local PDE problems and show the computed results in the global domain and on the interfaces. A significant component of our implementation is related to the computation of the updated values on the interfaces during iterations. These values need to be accurate enough to match the accuracy of the local discretization schemes. For this in each domain we compute the values of the function (u) and its partial derivatives (u_x, u_y) on a Cartesian mesh (MATLAB functions `tri2grid` and `gradient2`) and use the MATLAB function `interp2(. . . , 'spline')` to get u, u_x, u_y on the interfaces. Note that the meshes do not have to match on the interface lines and that `interp2` requires a Cartesian mesh. These values are then easily combined properly and are passed as new boundary conditions for the PDE problems involved in the next iteration.

In Fig. 6 we plot the contour lines of the experimentally estimated number of iterations required to reduce the max norm of the difference of two successive iterants below 10^{-5} as a function of the two relaxation parameters involved, ρ_1 and ρ_2. The stars in these plots denote the experimentally determined (by systematic search) optimum value of the relaxation parameters with which convergence is achieved in 14 and 15 iterations for PDE A and PDE B respectively. Unless otherwise stated, all numerical data presented in the rest of this section were obtained using as values for the relaxation parameters ρ_1 and ρ_2 the center of the convergence region (15) theoretically determined for the associated "1-dimensional" decomposition problem. This choice appears to be relatively "close" to optimum in all cases considered. We note that the convergence region shrinks by a factor of approximately 5 as we move from the 1- to the 2-dimensional case. Such behavior has been observed in other iterative schemes too.

We next plot in Fig. 7, in a way similar to the one used in the 1-dimensional case in Fig. 5, the convergence history. Specifically we plot the max norm of the relative difference of two successive iterants on the two interface points as is depicted by the legends on the left versus the number of iterations. We easily arrive at the conclusion that the rate of convergence is independent of the local discretization resolution h and depends very little on the PDE coefficient γ^2.

In an effort to obtain an inside picture about the characteristics of the convergence of the **GEO** method for 2-dimensional problems we present plots of the exact solution and the computed solutions on the whole domain at iterations 1, 3 and 10 in Fig. 9 and on the interface point at iterations 1, 2, 3 and 10 in Fig. 10. We easily see that the high frequency components of the error are cut off during the first iterations. We also observe the smooth and monotone type of convergence on the interfaces.

6. Conclusions

The main objective of this paper was to prove and elucidate the convergence characteristics of the **GEO** interface relaxation method for simple 1-dimensional problems mainly through a theoretical analysis on both the discrete (Linear Algebra) and the continuous (PDE) levels. In particular we have obtained analytical expressions for the relaxation parameters involved and hence the associated rate of convergence. These expressions in both their continuous (Theorem 3) and discrete (Theorem 8) forms relate the relation of the IR method with the various parameters of the differential problem, namely

[2] http://www.mathworks.com/products/pde/.

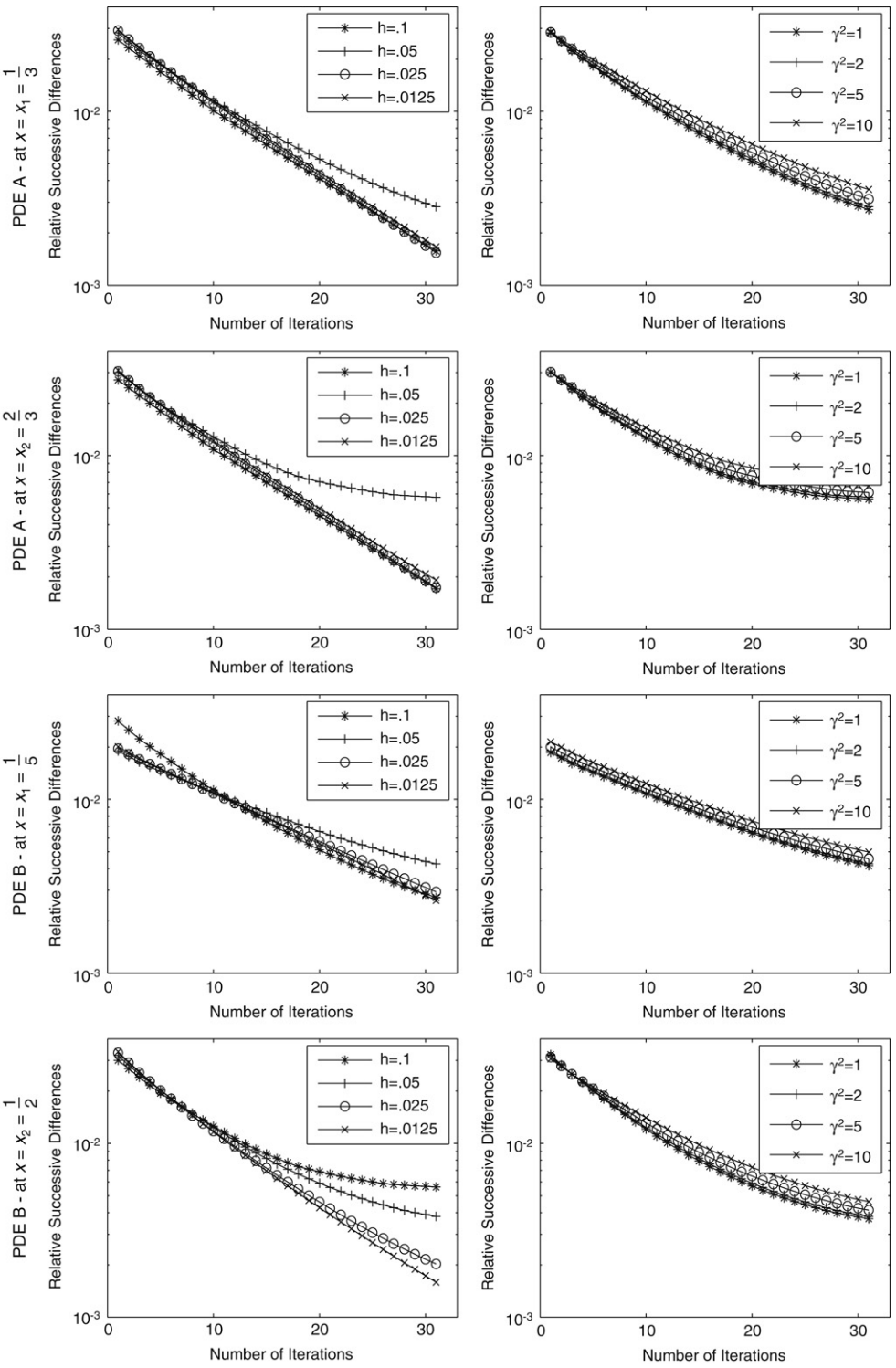

Fig. 7. Plots of max norm of the relative difference of two successive iterants measured at the two interfaces of the two problems PDE A and PDE B versus the number of iterations. For the plots on the left we set $\gamma^2 = 2$ and $h = 0.1/(2^i)$ for $i = 0, 1, 2, 3$ and for the plots on the right $\gamma^2 = 1, 2, 5, 10$ and $h = .05$.

the coefficients γ_i's and the length of each subdomain ℓ_i, and exhibit both the effectiveness (rate of convergence) and applicability (regions of convergence) of the method. The agreement of the two theoretical approaches is clearly seen, while the numerical experiments confirm the theoretical results.

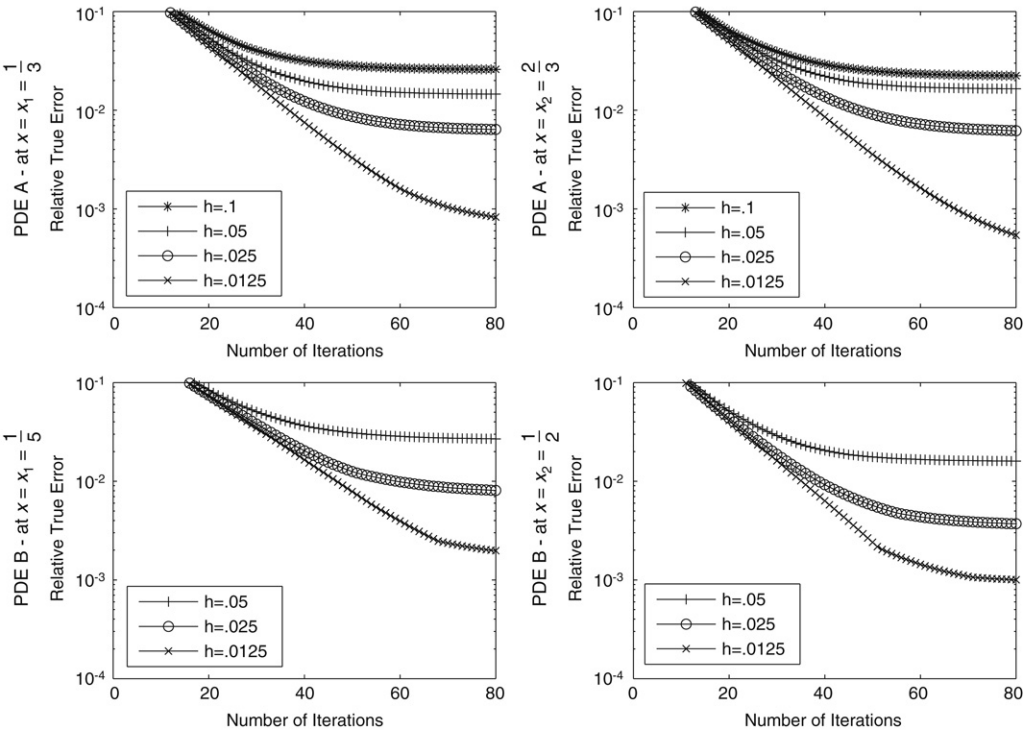

Fig. 8. Plots of max norm of the relative true error of the computed solution $\|u^{(k)} - u\|/\|u\|$ versus the iteration number k for the configurations considered in Fig. 7.

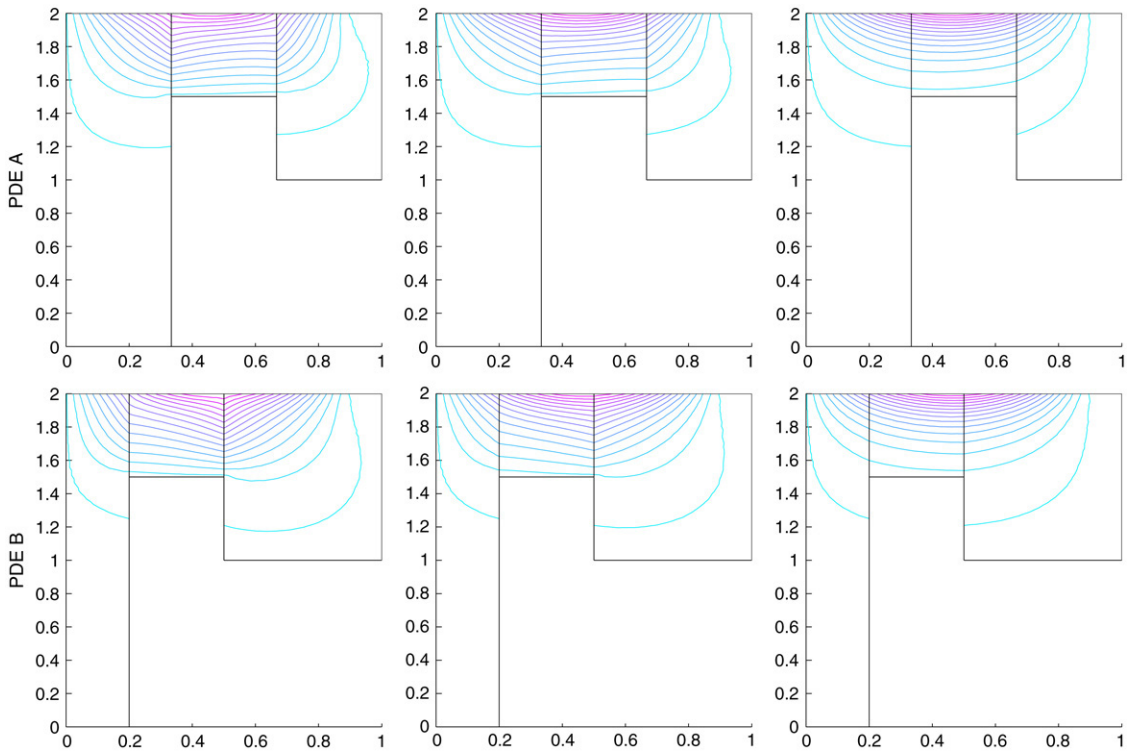

Fig. 9. Contour plots of the computed solution at iterations $k = 1$, 3 and 10 for the two PDE problems.

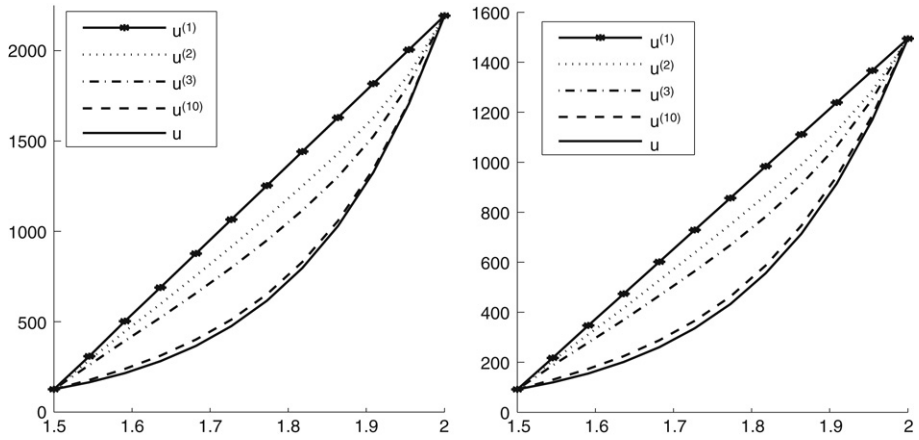

Fig. 10. Plots of the true solution and the computed solution on the interfaces at iterations $k = 1, 3, 10$ for the two PDE problems.

GEO exhibits desirable converge behavior while the fact that its rate of convergence is independent of the local discretization step is its most important feature. Our theoretical and experimental analyses clearly show that the convergence of the method depends (besides the physical parameters of the PDE problem) only on the relaxation parameters ρ_i. The various theoretical results presented in Sections 3 and 4 provide us with mechanisms for selecting proper (or optimal) values for these relaxation parameters. An additional/alternative mechanism for fine tuning the **GEO** method, at a higher conceptual level and for higher-dimensional problems, could be provided by the discussion related to Fig. 1 and the definition of the ρ_i's in terms of the w_i's (see Section 2). These w_i's denote the validity of the slope of the (computed) solution on the interface and there is a possibility that they might be either computationally estimated or determined through the properties of the mathematical model or the associated physical problem. Such fine tuning mechanisms are currently under development. In general, we may view **GEO** as a basic iteration scheme (just like the SOR for algebraic linear systems) that in some cases is not as fast as desired and which can be accelerated though mechanisms like the one mentioned above or be used as a preconditioner to rapidly converging schemes (like SSOR or AOR for the Conjugate Gradient method in the case of algebraic equations).

The in-depth understanding of the **GEO** method for 2- and 3-dimensional PDEs is still an open problem. For example, the analysis of a generalized **GEO** scheme which involves relaxation parameters that are functions of the space variables will certainly improve the capabilities of the method. Such a theoretical analysis is challenging and surely beyond the scope of this paper.

For further reading

Fig. 8, [2].

References

[1] J. Boloni, D.C. Marinescu, J.R. Rice, P. Tsompanopoulou, E. Vavalis, Agent based scientific simulation and modeling, Concurrency: Practice and Experience 12 (2000) 845–861.
[2] T. Drashansky, An agent-based approach to building multidisciplinary problem solving environments, Ph.D. Thesis, Purdue University, Computer Science Department, 1996.
[3] P. Henrici, Applied and Computational Complex Analysis, John Wiley, New York, NY, 1974.
[4] E.N. Houstis, A.C. Catlin, P. Tsompanopoulou, D. Gottfried, G. Balakrishnan, K. Su, J.R. Rice, Gasturbnlab: A multidisciplinary problem solving environment for gas turbine engine design on a network of non-homogeneous machines, Journal of Computational and Applied Mathematics 149 (1) (2002) 83–100.
[5] P.L. Lions, On the Schwarz alternating method III: A variant for nonoverlapping subdomains, in: R. Glowinski, G.H. Golub, G.A. Meurant, J. Periaux (Eds.), Domain Decomposition Methods for Partial Differential Equations, SIAM, 1990, pp. 202–223.
[6] S. Markus, E. Houstis, A. Catlin, J. Rice, P. Tsompanopoulou, E. Vavalis, D. Gottfried, K. Su, G. Balakrishnan, An agent-based netcentric framework for multidisciplinary problem solving environments, International Journal of Computational Engineering Science 1 (2000) 33–60.
[7] H.S. McFaddin, J.R. Rice, Collaborating pde solvers, Applied Numerical Mathematics (1992) 279–295.
[8] M. Mu, Solving composite problems with interface relaxation, SIAM Journal on Scientific Computing 20 (1999) 1394–1416.
[9] M. Mu, J.R. Rice, Modeling with collaborating PDE solvers—theory and practice, Computing Systems in Engineering 6 (1995) 87–95.
[10] J.R. Rice, An agent-based architecture for solving partial differential equations, SIAM News 31 (6) (1998).
[11] J.R. Rice, P. Tsompanopoulou, E. Vavalis, Interface relaxation methods for elliptic differential equations, Applied Numerical Methods 32 (2000) 219–245.
[12] J.R. Rice, P. Tsompanopoulou, E. Vavalis, Fine tuning interface relaxation methods for elliptic differential equations, Applied Numerical Methods 43 (2002) 459–481.
[13] J.R. Rice, E. Vavalis, D. Yang, Analysis of a non-overlapping domain decomposition method for elliptic PDEs, Journal of Computational and Applied Mathematics 87 (1998) 11–19.

[14] P. Tsompanopoulou, E. Vavalis, An experimental study of interface relaxation methods for composite elliptic differential equations, Applied Mathematical Modelling 23 (2008) 1620–1641.
[15] R.S. Varga, Matrix Iterative Analysis, Prentice-Hall, Inc, New Jersey, 1962.
[16] E. Vavalis, A collaborating framework for air pollution simulations, in: NATO-ASI Series, 1999, pp. 349–358.
[17] E. Vavalis, Runtime support for collaborative air pollution agents, Systems Analysis Modeling Simulation 42 (2002) 1575–1600.
[18] O. von Estorff, C. Hagen, Iterative coupling of FEM and BEM in 3D transient elastodynamics, Engineering Analysis with Boundary Elements 30 (7) (2006) 611–622.